

# Broadband field-resolved terahertz detection via laser induced air plasma with controlled optical bias

Chia-Yeh Li,<sup>1,\*</sup> Denis V. Seletskiy,<sup>1,2</sup> Zhou Yang,<sup>1</sup> and Mansoor Sheik-Bahae<sup>1,3</sup>

<sup>1</sup>Department of Physics and Astronomy, University Of New Mexico, Albuquerque, New Mexico, USA

<sup>2</sup>Department of Physics and Center for Applied Photonics, University of Konstanz D-78457 Konstanz, Germany

<sup>3</sup>msb@unm.edu

\*cyl@unm.edu

**Abstract:** We report a robust method of coherent detection of broadband THz pulses using terahertz induced second-harmonic (TISH) generation in a laser induced air plasma together with a controlled second harmonic optical bias. We discuss a role of the bias field and its phase in the process of coherent detection. Phase-matching considerations subject to plasma dispersion are also examined.

©2015 Optical Society of America

**OCIS codes:** (300.6495) Spectroscopy, terahertz; (040.2235) Far infrared or terahertz; (300.6500) Spectroscopy, time-resolved; (300.6530) Spectroscopy, ultrafast.

---

## References and links

1. Q. Wu and X.-C. Zhang, "Free-space electro-optic sampling of terahertz beams," *Appl. Phys. Lett.* **67**(24), 3523–3525 (1995).
2. P. R. Smith, D. H. Auston, and M. C. Nuss, "Subpicosecond photoconductive dipole antennas," *IEEE J. Quantum Electron.* **24**(2), 255–260 (1988).
3. M. van Exter and D. R. Grischkowsky, "Characterization of an optoelectronic terahertz beam system," *IEEE Trans. Microw. Theory Tech.* **38**(11), 1684–1691 (1990).
4. A. Nahata, A. S. Weling, and T. F. Heinz, "A wideband coherent terahertz spectroscopy system using optical rectification and electro-optic sampling," *Appl. Phys. Lett.* **69**(16), 2321–2323 (1996).
5. A. Leitenstorfer, S. Hunsche, J. Shah, M. C. Nuss, and W. H. Knox, "Detectors and sources for ultrabroadband electro-optic sampling: experiment and theory," *Appl. Phys. Lett.* **74**(11), 1516–1518 (1999).
6. G. Gallot and D. Grischkowsky, "Electro-optic detection of terahertz radiation," *J. Opt. Soc. Am. B* **16**(8), 1204–1212 (1999).
7. A. Sell, R. Scheu, A. Leitenstorfer, and R. Huber, "Field-resolved detection of phase-locked infrared transients from a compact Er:fiber system tunable between 55 and 107 THz," *Appl. Phys. Lett.* **93**(25), 251107 (2008).
8. B. Ferguson and X.-C. Zhang, "Materials for terahertz science and technology," *Nat. Mater.* **1**(1), 26–33 (2002).
9. A. Nahata and T. F. Heinz, "Detection of freely propagating terahertz radiation by use of optical second-harmonic generation," *Opt. Lett.* **23**(1), 67–69 (1998).
10. H. Hamster, A. Sullivan, S. Gordon, W. White, and R. W. Falcone, "Subpicosecond, electromagnetic pulses from intense laser-plasma interaction," *Phys. Rev. Lett.* **71**(17), 2725–2728 (1993).
11. D. J. Cook and R. M. Hochstrasser, "Intense terahertz pulses by four-wave rectification in air," *Opt. Lett.* **25**(16), 1210–1212 (2000).
12. X. Xie, J. Dai, and X.-C. Zhang, "Coherent control of THz wave generation in ambient air," *Phys. Rev. Lett.* **96**(7), 075005 (2006).
13. M. Kress, T. Löffler, S. Eden, M. Thomson, and H. G. Roskos, "Terahertz-pulse generation by photoionization of air with laser pulses composed of both fundamental and second-harmonic waves," *Opt. Lett.* **29**(10), 1120–1122 (2004).
14. K. Y. Kim, J. H. Glowonia, A. J. Taylor, and G. Rodriguez, "Terahertz emission from ultrafast ionizing air in symmetry-broken laser fields," *Opt. Express* **15**(8), 4577–4584 (2007).
15. K. Y. Kim, A. J. Taylor, J. H. Glowonia, and G. Rodriguez, "Coherent control of terahertz supercontinuum generation in ultrafast laser-gas interactions," *Nat. Photonics* **2**(10), 605–609 (2008).
16. J. Dai, X. Xie, and X.-C. Zhang, "Detection of broadband terahertz waves with a laser-induced plasma in gases," *Phys. Rev. Lett.* **97**(10), 103903 (2006).
17. N. Karpowicz, J. Dai, X. Lu, Y. Chen, M. Yamaguchi, H. Zhao, X.-C. Zhang, L. Zhang, C. Zhang, M. Price-Gallagher, C. Fletcher, O. Mamer, A. Lesimple, and K. Johnson, "Coherent heterodyne time-domain spectrometry covering the entire 'terahertz gap'," *Appl. Phys. Lett.* **92**(1), 011131 (2008).

18. Z. Lü, D. Zhang, C. Meng, L. Sun, Z. Zhou, Z. Zhao, and J. Yuan, "Polarization-sensitive air-biased-coherent-detection for terahertz wave," *Appl. Phys. Lett.* **101**(8), 081119 (2012).
19. H. Wang, K. Wang, J. Liu, H. Dai, and Z. Yang, "Theoretical research on terahertz air-breakdown coherent detection with the transient photocurrent model," *Opt. Express* **20**(17), 19264–19270 (2012).
20. M. Clerici, D. Faccio, L. Caspani, M. Peccianti, O. Yaakobi, B. E. Schmidt, M. Shalaby, F. Vidal, F. L'egar'e, T. Ozaki, and R. Morandotti, "Spectrally resolved wave-mixing between near- and far-infrared pulses in gas," *New J. Phys.* **15**(12), 125011 (2013).
21. H. Zhong, N. Karpowicz, and X.-C. Zhang, "Terahertz emission profile from laser-induced air plasma," *Appl. Phys. Lett.* **88**(26), 261103 (2006).
22. Y. S. You, T. I. Oh, and K. Y. Kim, "Off-axis phase-matched terahertz emission from two-color laser-induced plasma filaments," *Phys. Rev. Lett.* **109**(18), 183902 (2012).
23. I. Babushkin, S. Skupin, and J. Herrmann, "Generation of terahertz radiation from ionizing two-color laser pulses in Ar filled metallic hollow waveguides," *Opt. Express* **18**(9), 9658–9663 (2010).
24. X. Lu, N. Karpowicz, and X.-C. Zhang, "Broadband terahertz detection with selected gases," *J. Opt. Soc. Am. B* **26**(9), A66–A73 (2009).
25. R. W. Boyd, *Nonlinear Optics* (Academic, 2008).
26. Y. Minami, M. Nakajima, and T. Suemoto, "Effect of preformed plasma on terahertz-wave emission from the plasma generated by two-color laser pulses," *Phys. Rev. A* **83**(2), 023828 (2011).

---

## 1. Introduction

Most commonly used techniques for field-resolved measurement of terahertz radiation include electro-optic sampling (EOS) [1] and photoconductive response [2,3]. EOS relies on THz-induced linear Pockels effect, where transient birefringence, linearly proportional to the magnitude of the THz field, is time-resolved by a gating pulse. The bandwidth of this detection scheme is set by the mismatch of the phase velocity of the THz field and the group velocity of the gating pulse in the electro-optic crystal [4–6]. Ultrabroadband detection of THz radiation via EOS has been also demonstrated [7], however interpretation of the signal near the Reststrahlen band of the detector crystal requires some detailed corrections [5]. In the case of photoconductive detector, on the other hand, the bandwidth is ultimately limited by the non-instantaneous response of the carriers [8].

Third-order optical nonlinearity, i.e. a four-wave mixing process has also been used to detect THz radiation in a centrosymmetric solid-state media [9]. With the availability of millijoule near-infrared femtosecond pulses, it became possible to generate ultrabroad coherent THz emission from one [10] or two-color driven air-breakdown plasmas [11–13]. While requiring high input energies, the advantage of the gaseous medium is its potentially low dispersion together with an absence of the Reststrahlen band. The latter fact yields a smooth response function of the gas detector in comparison to solid-state EOS crystals, which require large corrections in the frequency range of approximately 5 – 10 THz [5]. While the full mechanism of THz generation in a plasma channel is generally described within the semi-classical plasma current model [14,15], it can be approximated as a third-order optical rectification [11–13], where two fundamental ( $E_{\omega}$ ) and one second harmonic ( $E_{2\omega}$ ) fields mix to produce THz output at the difference frequency. It should be noted that while the word "plasma" is often used here, it does not imply a stationary plasma nonlinearity, rather it involves the dynamic process of ionization followed by the acceleration of free electrons in the polar-asymmetric two-color field [14]. The generation process can be reversed for field-resolved broadband detection of THz transients. Analogous to the generation, air-biased coherent detection (ABCD) [16,17] is performed in a secondary (detection) channel, where THz and fundamental waves mix to produce terahertz-induced second harmonic (TISH) field. Field-resolved detection is then achieved by linear mixing of the TISH signal with a local oscillator (LO). In the first demonstration by Dai et al. [16], the local oscillator signal was derived from a second harmonic field produced in a supercontinuum of the detection plasma itself, which i) requires strong pulse energies for detection and ii) cannot be independently controlled both in terms of polarization, phase and bias intensity. A controlled LO was provided in a form of a high voltage DC bias across the detection plasma [17]. Here, the centro-symmetry of the medium is broken by the DC field, thus allowing for the generation of

second harmonic directly from the biased plasma. In such case, the requirement for high intensity probe pulse is relaxed along with the gained access to the polarization state of light via orthogonal high voltage electrode pairs [18], however at the expense of high voltage handling and inherited challenges of remote detection.

Here, we report a related yet modified detection method where we provide the required local oscillator optically. This is realized by insertion of a beta-barium borate ( $\beta$ -BBO) crystal in the path of the detection beam, before the generation point of the detection plasma. In our approach, the detection beam requires neither high intensity nor high voltage bias, while the intensity, phase and polarization of the  $2\omega$  can be precisely controlled, allowing field- and polarization-resolved measurements. The lack of high voltage in our scheme makes remote (stand-off) sensing more viable.

## 2. Formalism of the OBCD detection scheme

Terahertz induced second harmonic required for THz detection is generated by the reverse process of THz generation in a two-color driven gas plasma. The detection mechanism can either be treated by the plasma current model [14,15,19], or more commonly by the four-wave-mixing process [9] where  $I_{TISH} \propto |\chi^{(3)} E_\omega^2 E_{THz}|^2$ . In a time-resolved arrangement one measures a TISH signal that is a nonlinear cross correlation between the fundamental and the THz pulse

$$S_{TISH}(\tau) \propto \int |E_\omega^2(t+\tau)E_{THz}(t)|^2 dt. \quad (1)$$

According to Eq. (1), detected TISH signal is related to the instantaneous intensity of the THz field;  $E_{THz}$  cannot be obtained without a retrieval process [20]. Karpowicz et al. [17] introduced a DC-biased geometry where  $E_{THz}$  in Eq. (1) is replaced with  $E_{THz} + E_{dc}$ . Under this bias, a term  $\propto \text{Re}\left\{\int E_\omega^4(t+\tau)E_{dc}E_{THz}(t)dt\right\}$  can be extracted from Eq. (1) that gives a phase-resolved cross-correlation measurement of the THz field.

Field-resolved detection is equally possible by a linear mixing of the TISH signal with an optical (2nd harmonic) local oscillator  $E_{2\omega}^{LO}$ :

$$I_{2\omega} \propto |\chi^{(3)} E_\omega^2 E_{THz} + E_{2\omega}^{LO}|^2 = |\chi^{(3)} E_\omega^2 E_{THz}|^2 + |E_{2\omega}^{LO}|^2 + 2 \text{Re}\{\chi^{(3)} E_\omega^2 E_{THz} E_{2\omega}^{LO*}\}, \quad (2)$$

where now the third term has the desired linear proportionality to the applied  $E_{THz}$ . To ensure field-resolved detection, the contribution of the first two terms in Eq. (2) has to be minimized. The first term can be suppressed if  $|E_{2\omega}^{LO}|$  is much larger than the  $|E_{THz}|$ , and the second term which appears as a constant background can be experimentally excluded by lock-in detection. Under these conditions, the measured time-resolved cross-correlation signal reduces to

$$S_{2\omega}(\tau) \propto \text{Re}\left\{\int E_\omega^2(t)E_{2\omega}^{LO*}(t)E_{THz}(t+\tau)dt\right\}, \quad (3)$$

where detected signal now involves the  $E_{THz}$  field. The optical seeding is simpler to implement than the DC-biased plasma as it does not require a synchronized high-voltage pulse. However, as Eq. (3) suggests, this method is sensitive to the phases of optical beams since  $E_\omega^2(t)E_{2\omega}^{LO*}(t) = |E_\omega^2(t)||E_{2\omega}^{LO*}(t)|e^{i\Delta\phi}$ , where  $\Delta\phi = 2\phi_\omega - \phi_{2\omega}$  with  $\phi_\omega$  and  $\phi_{2\omega}$  denoting the phases of the fundamental and the second-harmonic bias, respectively. Since  $|E_{2\omega}^{LO*}(t)| \propto |E_\omega^2(t)| = I_\omega(t)$ , the measured signal is expected to vary as

$$S_{2\omega}(\tau) \propto \cos(\Delta\phi) \int I_\omega^2(t)E_{THz}(t+\tau)dt. \quad (4)$$

In this implementation, SH bias can be fully controlled (i.e. not generated in the supercontinuum), therefore providing a way to adjust the phase difference using dispersive optics to assure high sensitivity corresponding to  $\Delta\phi \sim m\pi$  ( $m = \text{integer}$ ). At the same time, direct access to the relative phase allows us to study the coherence of this detection scheme. Additionally, direct control of the intensity of the second harmonic bias field relaxes the requirement for high-intensity probe at a fundamental frequency, and the necessity of high voltage electronics is also removed. Similar to recently-reported two-electrode polarization-resolving ABCD scheme [18], the optically-biased coherent detection (OBCD) is also polarization sensitive. By properly rotating the polarization of the probe  $\omega$ , orthogonal polarization components of THz field can be time-resolved.

### 3. Experimental setup

Schematic of our experimental setup is depicted in Fig. 1. The laser source, 1kHz Ti:Sapphire regenerative amplifier with 35-fs pulse duration and maximum energy of 3.5 mJ, is split into two arms. One arm is used to generate a broadband single-cycle THz field [11–13], while the other is used to provide the detection plasma channel and our optical bias. For THz generation, near-infrared (NIR) pump beam is focused through a 30  $\mu\text{m}$  Type-I BBO crystal which produces the required two-color field at the output [11–13]. We ensure co-polarization of fundamental and second harmonic field with a true-zero-order half-wave plate (HWP) placed after the BBO. First order autocorrelation of the generated THz pulses reveals broad bandwidth with frequency components extending to 15 THz. The THz is then collimated and refocused onto the detection plasma with a pair of off-axis parabolic mirrors. Residual NIR pump and second harmonic are filtered by a high-resistivity silicon wafer, placed in the collimating portion of the telescope. With the measurements of average THz power a pyroelectric detector, THz spot size using a knife-edge technique and using the knowledge of the THz pulse duration, we estimate the THz field strength to be  $\sim 1$  MV/cm at the focus of the second paraboloid.

The probe pulse of 50  $\mu\text{J}$  energy was focused by a lens with a 175 mm focal length through a hole in second paraboloid to generate detection plasma in spatio-temporal overlap with the focus of the THz. Since spectral and spatial THz profile from the plasma is not uniform [21,22], a 5-mm long stainless steel cylindrical waveguide of inner diameter  $< 200$   $\mu\text{m}$  is placed near the focus to improve phase matching with THz frequencies of large  $k$  vector [23]. HWP is used to control polarization of the fundamental and a 10  $\mu\text{m}$ -thick Type-I BBO is used to generate the controlled  $2\omega$  bias. As was already discussed with Eq. (4), the OBCD signal depends on the relative phase difference  $\Delta\phi$  between the fundamental and the  $2\omega$  bias. This parameter can be controlled by inserting a dispersive element such as a thin fused silica plate or a pair of wedges, after the optical bias generation in the detection arm. If the two beams are kept at the cross-polarization state (due to type-I phase matching), a calcite plate can be used instead to induce the desired phase delay, as shown in Fig. 1. In this case, the birefringence in calcite is further exploited to temporally advance the  $2\omega$  bias envelope in order to eliminate any potential pulse distortion that may arise from propagation in the air plasma. A second complementary calcite plate is then used after the plasma to synchronize the TISH and the  $2\omega$  bias pulses. The interference between the two cross-polarized pulses is achieved using an adjustable analyzer with precise control over their relative amplitudes.

Detection of the interference signal, as depicted in Eq. (4), is accomplished with a NIR-blind photo-multiplier tube (PMT) after a 400 nm band-pass filter (BP, Fig. 1) to suppress background counts due to detection of any unwanted spectral components. Mechanical chopper at the generation arm and lock-in detection are utilized to ensure that predominantly field-dependent TISH component is detected (see Section 2).

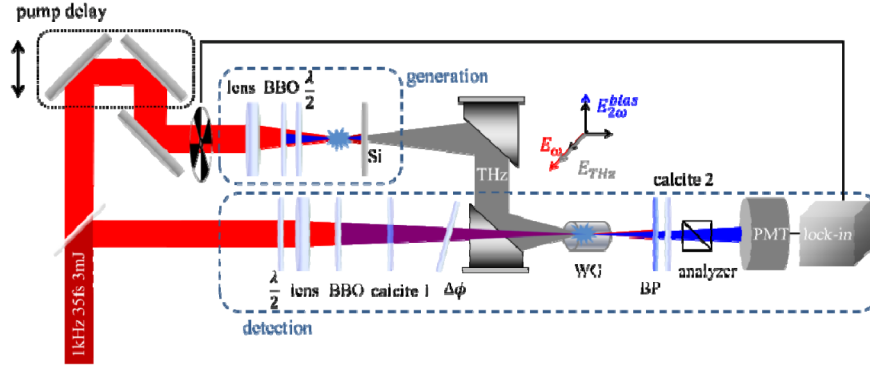


Fig. 1. Experimental setup for optically-biased coherent detection (OBCD) consists of two arms where generated THz (using a two-color driven gas plasma, see “lens” + “BBO” + “ $\lambda/2$ ” plate) is field-resolved in a detection plasma (see “ $\lambda/2$ ” plate + “lens” + “BBO” + “calcite” plate + waveguide “WG” depicted in are encircled by rectangle marked “detection”) by means of a  $2\omega$  bias, acting as a local oscillator for coherent detection. Interference signal (see Eq. (4)) is detected after a bandpass filter (BP) by a photomultiplier tube (PMT) and a lockin amplifier.

#### 4. Results and discussion

Typical OBCD time traces of a field-resolved THz transient are shown in Fig. 2(a). With mechanical chopping frequency of 370 Hz, 100 ms lock-in integration time constant, and averaging over three waveforms, the signal-to-noise ratio is approximately 40 to 1. The ultrafast transient contains frequency components extending beyond 10 THz, as shown in Fig. 2(b), consistent with the results of linear autocorrelation measurements. Oscillations after the trailing edge of the pulse correspond to a free-induction decay of coherently-excited resonances in water vapor and can be removed with a proper purge of the setup with dry air.

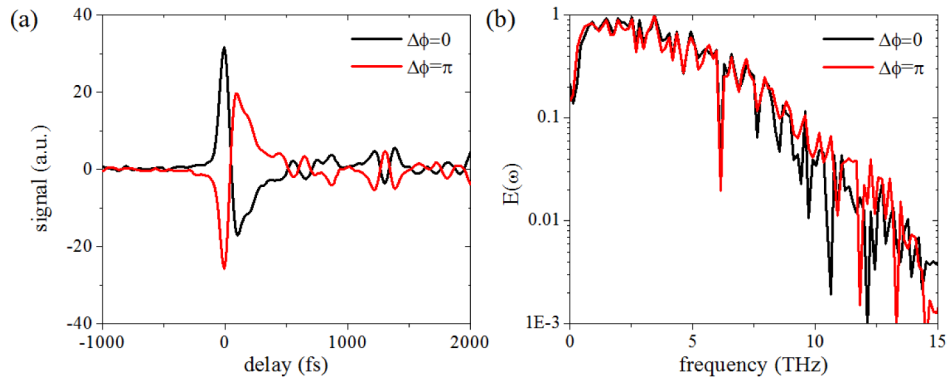


Fig. 2. (a) Time-resolved broadband THz field transients detected with the OBCD method with  $0$  and  $\pi$  relative phase shift between the probe  $\omega$  and the optical bias  $2\omega$  fields. Nearly perfect change of polarity of the field attests to fully coherent detection method. (b) The corresponding spectrum of a field-resolved OBCD detection method for  $\Delta\phi = 0$  and  $\Delta\phi = \pi$ .

We first verified the possibility to control the phase of the detected signal by changing  $\Delta\phi$  by  $\pi$ , as shown in Fig. 2(a). Here the maximum obtainable signal is denoted as  $\Delta\phi = 0$ , due to the assumption that TISH is generated by a four-wave mixing process, as discussed in Section 2. The observed change of polarity matches exactly the expected behavior predicted by Eq. (4), providing a direct control over the maximum obtainable signal and a convenient method of relative phase calibration.

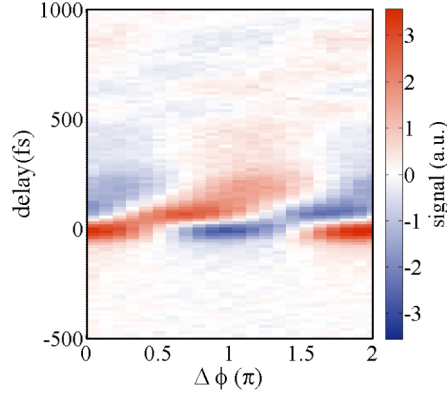


Fig. 3. Measured OBCD signal  $S(\tau, \Delta\phi)$ .

The entire mapping of  $S(\Delta\phi, t)$  is also obtained, as shown in Fig. 3. The most notable feature is the expected  $2\pi$  periodicity of the coherent signal as a function of the relative phase. Interestingly, the signal does not show a node at  $\Delta\phi = \pi/2$ , as expected from Eq. (4). To explain this feature, we realize that the measured TISH spectrum is slightly redshifted compared to the bias SH which is centered at  $2\omega$ , as shown in Fig. 4. This frequency shift is a consequence of phase matching considerations for tightly focused Gaussian beams [24,25]. Assuming a four-wave mixing model, the TISH generation may involve two parametric processes given by  $\omega_{TISH}^{\pm} = 2\omega \pm \omega_{THz}$ . However, as also suggested by Lu et al, in the presence of normal dispersion, the phase-matching requirements under the Gouy phase of the interacting Gaussian beams strongly favor the  $\omega_{TISH}^{-} = 2\omega - \omega_{THz}$  process [20,24]. Using standard formalism governing four-wave-mixing of Gaussian beams [24,25], we evaluated the TISH spectrum subject to propagation in a plasma with refractive index  $n_{plasma} = \sqrt{1 - \omega_p^2 / \omega^2}$ , with the plasma frequency  $\omega_p = \sqrt{n_e e^2 / m_e \epsilon_0}$  and  $n_e$ ,  $e$ ,  $m_e$ , and  $\epsilon_0$  being number density of electron, electric charge, mass of electron, and permittivity of free space, respectively. Since propagation of electromagnetic waves is forbidden (or heavily damped) at  $\omega < \omega_p$ , both THz and TISH generation must occur primarily in underdense (partially ionized) spatio-temporal regions of the air-breakdown plasma [26]. This corresponds to a plasma cone that forms as the front of the excitation pulse propagates and ionizes the air in the focal region. To estimate the phase-matching conditions due to plasma dispersion, we took  $\nu_{THz} \sim 8$  THz and assumed  $\nu_p \sim 1.3$  THz as suggested by the observed low-frequency cut-off in Fig. 2(b). As shown in Fig. 4, the calculated TISH spectrum exhibits the redshifting as observed experimentally.

We analytically examine the effect of this mismatch of central wavelengths between the bias and TISH fields as well as of finite probe duration on the  $S(\Delta\phi, \tau)$  map. Assuming a frequency mismatch of  $\Delta\omega$  between TISH and  $2\omega$ -bias, the cross-correlation signal produced by Eq. (3) is now:

$$S_{2\omega}(\tau) \propto \int I_{\omega}^2(t) E_{THz}(t + \tau) \cos(\Delta\phi + \Delta\omega t) dt. \quad (5)$$

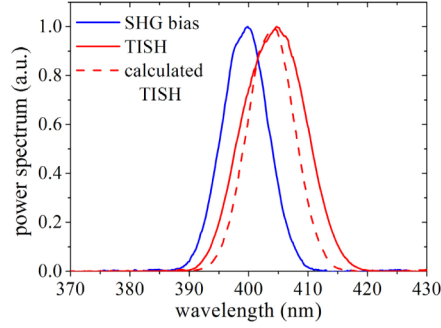


Fig. 4. Measured (solid line) and calculated (dashed line) TISH and measured bias SHG spectra at zero delay. Phase-matching is considered for center frequency of 8 THz. The redshifted TISH spectrum demonstrates the dominance of the  $\omega_{TISH}^- = 2\omega - \omega_{THz}$  process, see text for additional details.

Equation (5) shows that the mismatch in carrier frequencies of the bias and TISH fields essentially manifests itself as a delay-dependent phase shift, consistent with the observation in Fig. 3. Figure 5 shows the numerical simulation of  $S(\Delta\phi, \tau)$  under no shift ( $\Delta\omega = 0$ ) and a finite and negative  $\Delta\omega$ , corresponding to  $\sim 4$  nm redshift as deduced experimentally. The calculation captures the essential features observed in the experiment, as seen in comparison of Fig. 3 and Fig. 5(b). Small qualitative differences in the measured and calculated maps are likely due to the assumption of constant TISH central wavelength throughout the delay.

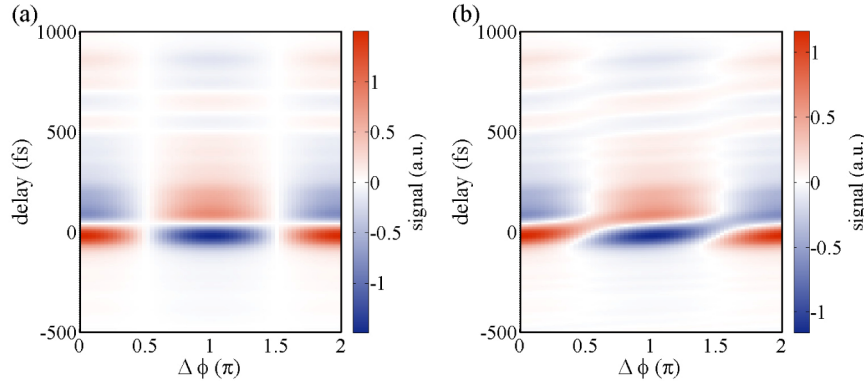


Fig. 5. Calculated OBCD signal  $S(\Delta\phi, \tau)$  using Eq. (5) and assuming the THz filed from Fig. 2: (a) without and (b) with the TISH center wavelength shift of 4 nm.

Finally, it is important to point out that the preferred phase-matching condition resulting in redshifted TISH spectrum shows pronounced effects in the  $S(\Delta\phi, \tau)$  map only around the nodes given by  $\Delta\phi = (2m+1)\pi/2$ . This in turn implies that the OBCD signal read out at  $\Delta\phi = m\pi$  is minimally affected by the phase-matching condition, so long as the frequency shift does not exceed approximately FWHM of the injected SH bias spectrum. Thus, the ability to independently adjust the relative phase of the bias field proves important in achieving correct coherent measurement of the  $E_{THz}$  profile at  $\Delta\phi = m\pi$ .

## 5. Summary

We have demonstrated the Optically Biased Coherent Detection (OBCD) of THz pulses using THz-induced second harmonic generation in laser induced plasma under injection of phase-controlled second harmonic bias beam. The effect of phase relationship between probe

fundamental and second harmonic bias has been investigated. The variation of cross-correlation data with coherent phase and the delay are attributed to the red-shifted TISH spectrum as a consequence of phase-matching conditions and plasma dispersion. Despite this variation, we nonetheless conclude that the detection correctly reproduces coherent profile of the THz field for certain values of the relative phase, underscoring the importance of its control. In addition, the controlled optical bias has several benefits including the relaxed requirement for high energy pulses and high voltages, making OBCD potentially viable for broadband terahertz stand-off detection. All-optical method with full access to phase and polarization of the bias field yields direct routes for optimization and polarization sensitive detection.

### **Acknowledgments**

The funding of this research was partially provided by Nation Science Foundation (NSF) Award DMR-1207489, and Defense Threat Reduction Agency (DTRA). D.V.S. also acknowledges partial support by the National Science Foundation under Award No. 1160764 and ZIF-Marie-Curie project (FP7-PEOPLE Program of Marie Curie Actions).